Efficiency of cellular uptake of nanoparticles via receptor-mediated endocytosis

Anand Banerjee,[1] Alexander Berzhkovskii,[2] and Ralph Nossal[1]

[1]*Program in Physical Biology, Eunice Kennedy Shriver National Institute of Child Health, and Human Development, National Institutes of Health, Bethesda, Maryland 20892, USA*

[2]*Mathematical and Statistical Computing Laboratory, Division of Computational Bioscience, Center for Information Technology, National Institutes of Health, Bethesda, Maryland 20892, USA*

(Dated: November 27, 2014)

Abstract

Experiments show that cellular uptake of nanoparticles, via receptor-mediated endocytosis, strongly depends on nanoparticle size. There is an optimal size, approximately 50 nm in diameter, at which cellular uptake is the highest. In addition, there is a maximum size, approximately 200 nm, beyond which uptake via receptor-mediated endocytosis does not occur. By comparing results from different experiments, we found that these sizes weakly depend on the type of cells, nanoparticles, and ligands used in the experiments. Here, we argue that these observations are consequences of the energetics and assembly dynamics of the protein coat that forms on the cytoplasmic side of the outer cell membrane during receptor-mediated endocytosis. Specifically, we show that the energetics of coat formation imposes an upper bound on the size of the nanoparticles that can be internalized, whereas the nanoparticle-size-dependent dynamics of coat assembly results in the optimal nanoparticle size. The weak dependence of the optimal and maximum sizes on cell-nanoparticle-ligand type also follows naturally from our analysis.

email - banerjeea3@mail.nih.gov

INTRODUCTION

In recent years there has been great interest in using nanoparticles (NPs) for various biomedical applications including imaging, biosensing, and targeted gene/drug delivery (see review articles [1–3] and references therein). Successful realization of these applications requires efficient cellular uptake of the NPs. To this end, the NPs are coated with ligands that allow them to bind to specific cell surface receptors and be internalized via receptor-mediated endocytosis. An understanding of how the physical properties of NPs, like their size, shape, charge, etc., affect the internalization process is crucial for designing NPs for biomedical purposes.

Experiments show that the NP size is an important parameter that determines the mechanism of their cellular uptake. In particular, NPs smaller than approximately 200 nm are internalized typically via receptor-mediated endocytosis whereas, for larger NPs other mechanisms are involved [4, 5]. Furthermore, the uptake rate of the NPs, that are internalized via receptor-mediated endocytosis, is strongly size dependent. There is an optimal NP size, approximately 50 nm in diameter, at which the uptake rate is highest [4–11]. In Table I we collected data from various experiments designed to study size dependence of NP uptake. The experiments were performed using different kinds of cell lines, NPs, and ligands; yet the optimal size was found to be approximately the same. This surprising observation suggests that the optimal size weakly depends on the above mentioned factors.

Several theoretical models of receptor-mediated endocytosis of NPs have been proposed in the literature [12–16]. A common feature of these models is that they assume the uptake is controlled by the formation of chemical bonds between receptors on the cell surface and ligands attached to the NP. Using such an approach these studies conclude that the optimal NP size is a function of the receptor density on the cell membrane, ligand density on the NP, and the receptor-ligand binding energy. These parameters however can change significantly depending on the cell line and ligands used in the experiment. Therefore, in the framework of these models, it is difficult to explain the same optimal size observed in different experiments. Furthermore, such an approach leads to the prediction that even micron sized NPs can be internalized via receptor-mediated endocytosis [12, 13] which has never been observed experimentally.

Along with the formation of chemical bonds between the NP ligands and cell surface

receptors, receptor-mediated endocytosis involves the assembly of a protein coat on the cytoplasmic side of the outer cell membrane. In the case of clathrin-mediated endocytosis - which is a form of receptor-mediated endocytosis - the coat contains several proteins including clathrin, adaptor proteins, membrane bending proteins like epsin, amphiphysin, etc.[17, 18]. The coat assembly plays a vital role in internalization of cargo, and any interference with this process drastically reduces the endocytic capacity of a cell. For example, cellular uptake of NPs is significantly reduced when the cells are pretreated with sucrose or potassium-depleted medium [4, 19], which are known to disrupt coat formation. The above mentioned models do not take the coat assembly into explicit consideration. Therefore, how this key aspect of the cellular endocytic machinery affects the uptake of NPs remains to be elucidated.

In this paper we make a step in this direction. Our main purpose is to demonstrate that, contrary to the current understanding, the size-dependence of cellular uptake of NPs is determined by the coat assembly. To do so, we use a previously developed coarse-grained model of the coat assembly that focuses on vesicle formation during clathrin-mediated endocytosis [20]. The model was developed to explain the fates and lifetimes of clathrin coated

TABLE I: Summary of experimental results on the size dependence of cellular uptake of NPs. NPs smaller than 200 nm are internalized via receptor-mediated endocytosis, whereas for larger NPs other internalization mechanisms are involved [4, 5]. Bold faced numbers indicate the NP size for which the cellular uptake is highest.

Cells	NP type	Ligand	NP size (diameter nm)	Ref.
B16-F10	Latex beads	No ligand	**50**,100,200,500	4
MNNG/HOS	Metal hydroxide	Not specified	**50**,100,200,350	5
Hela	Quantum dots	Not specified	5,15,**50**	6
Hela, STO, SNB19	Gold	Transferrin	14,30,**50**,74,100	7
CL1-0, Hela	Gold	single-stranded DNA	**45**,75,110	8
HeLa	Mesoporous silica	Not specified	30,**50**,110,170,280	9
A549, HeLa, MDA	Gold	Transferrin	15,30,**45**	10
Caco-2	Liposomes	Not specified	**40**,72,86,97,162	11

pits (CCPs); here we use it to study the size dependence of NP uptake. In particular, we calculate the dependence of the NP internalization probability and the internalization time on the NP size. Our results show that the above-mentioned experimental observations, namely, (1) the optimal NP size, (2) an upper bound on the size of NPs that can be internalized, and (3) the weak dependence of these sizes on type of cells, NPs, and ligands used in different experiments, can be understood to be the consequence of the dynamics of coat assembly. This is the main result of our work.

MODEL

We start by describing the main steps involved in NP internalization via clathrin-mediated endocytosis. During clathrin-mediated endocytosis a ligand-coated NP first binds to a specific receptor on the surface of the cell membrane (see Fig. 1). After binding, the NP-receptor complex binds adaptor proteins (typically AP-2), which recruit other endocytic proteins, and clathrin-coated pit (CCP) assembly begins. CCP assembly is a stochastic process which has two possible final outcomes [21, 22]. One is that the CCP grows in size and forms a vesicle, in which case the NP is completely wrapped and internalized. The other possibility is that the CCP grows only up to a certain size and then disassembles. In this case the

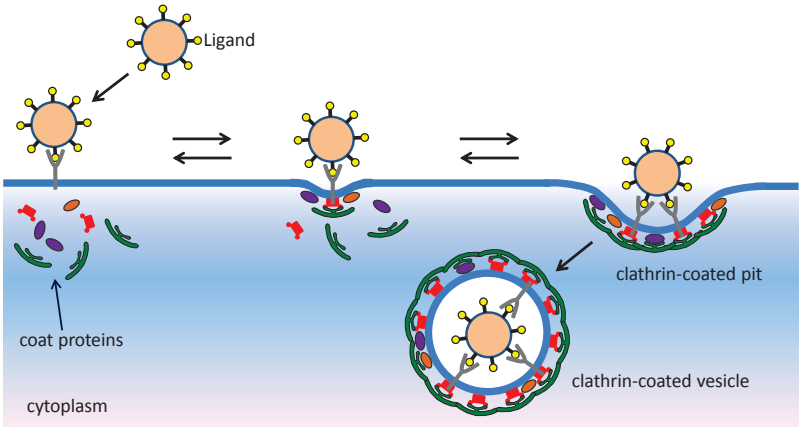

FIG. 1: Schematic diagram of NP internalization via clathrin-mediated endocytosis. A NP first binds to a specific cell surface receptor forming a NP-receptor complex. The complex binds the coat proteins and CCP assembly begins. The CCP either grows to form a vesicle, in which case the NP is internalized, or grows only up to a certain size and then disassembles.

NP-receptor complex becomes free of coat proteins, and the assembly process starts once again. We assume that the binding of a NP to the cell membrane is irreversible, and that the dissociation of the NP-receptor complex may be neglected. We discuss the restrictions of this assumption below.

Quantifying internalization efficiency

Similar to other approaches [12, 15], we characterize the NP internalization efficiency by the mean internalization time, τ, defined as the mean time between the binding of a NP to the membrane and its internalization. As shown in Appendix A,

$$\tau = \tau_w + (\tau_0 + P_f \tau_f)/P_w, \tag{1}$$

where τ_0 is the mean time required for the initiation of CCP assembly around a free NP-receptor complex, P_w and $P_f = 1 - P_w$ denote the probabilities of successful and unsuccessful wrapping of a NP, and τ_w and τ_f denote the mean durations of these processes. Here w and f indicate successful and failed wrapping of the NP, respectively. Our assumption that the NP-receptor dissociation may be neglected is valid if P_w is not too small. Otherwise, τ becomes very large, and the dissociation of the complex should be taken into consideration.

In order to calculate the quantities appearing in Eq. 1 we use the model of CCP assembly developed in Ref. 20. Here we briefly describe the model and list the underlying assumptions. As mentioned earlier the coat that forms during CCP assembly contains several proteins and has a complex structure. Proteins like epsin and amphyphysin bind directly to the cell membrane and impart a local curvature; whereas clathrin triskelions (three-legged, pinwheel-wheel shaped complexes) bind with other clathrin triskelions to form a three-dimensional scaffold which is linked to the membrane through the adaptor proteins (typically AP-2). The clathrin scaffold imparts global curvature to the cell membrane. Incorporating this complex structure of the coat into a model is an extremely complicated task. To overcome this difficulty, in Ref. 20 we proposed a coarse-grained description of CCP assembly. The main idea was to replace the real protein coat by a coat made up of identical units referred to as monomers (Fig. 2). We assumed that (1) the coat made up of monomers has its own bending rigidity and a spontaneous curvature, (2) the shape of the model CCP (pit) is a spherical cap, (3) the monomers are structureless, which means that at the time of binding

the orientation of a monomer is not important. Due to these assumptions certain details of CCP assembly were lost, but this is the price we had to pay for a tractable model which still contained the essential features of the assembly process. We validated this model by showing that it was capable of explaining the experimentally measured lifetime distribution of CCPs [20]. Similar coarse-grained approaches for modeling the protein coat have been used in Refs. 23 and 24 for studying endocytic vesicle formation in yeast and COP vesicle formation in the Golgi, respectively.

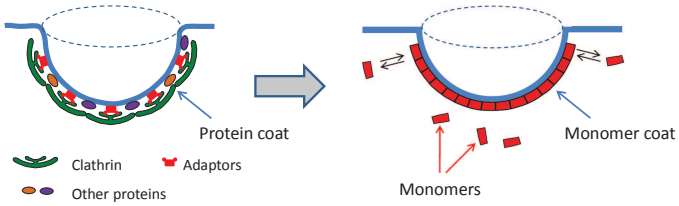

FIG. 2: Coarse-grained model of a clathrin-coated pit (CCP). In a real CCP the protein coat contains clathrin and several other proteins. The model coat is made of identical monomeric units. The shape of the model CCP is assumed to be a spherical cap, and the average area of a monomer is chosen to be the same as that occupied by a clathrin triskelion in a real CCP.

Using the coarse-grained model of CCP discussed above, the dynamics of CCP assembly around a NP-receptor complex can be described by the kinetic scheme shown in Fig. 3. In this kinetic scheme the symbol n is the number of monomers in a pit that forms around the NP-receptor complex, and N is the number of monomers needed for a complete vesicle. N is related to the NP diameter d_{NP} by the relationship

$$N = \pi(d_{NP} + 2l_b)^2/\lambda, \tag{2}$$

where l_b is the typical length of the receptor-ligand bond between the NP and the cell

$$0 \underset{\beta_1}{\overset{k_0}{\rightleftarrows}} 1 \underset{\beta_2}{\overset{\alpha_1}{\rightleftarrows}} 2 \underset{\beta_3}{\overset{\alpha_2}{\rightleftarrows}} \cdots \underset{\beta_n}{\overset{\alpha_{n-1}}{\rightleftarrows}} n \underset{\beta_{n+1}}{\overset{\alpha_n}{\rightleftarrows}} \cdots \underset{\beta_N}{\overset{\alpha_{N-1}}{\rightleftarrows}} N \xrightarrow{k_N}$$

FIG. 3: Kinetic scheme of pit assembly. Symbols n, and N refer to the number of monomers in a pit and a vesicle, respectively. The rate constants α_n and β_n characterize the growth and decay rates of a pit of size n. k_0 is the rate at which the first monomer binds to the NP-receptor complex, and k_N is the rate of scission of a vesicle from the membrane.

membrane, and λ is the average area occupied by a monomer. The rate constants α_n and β_n characterize the growth and decay rates of a pit of size n, $k_0 = 1/\tau_0$ is the rate constant for binding of the first monomer to the NP-receptor complex, and k_N is the rate constant for the scission of a vesicle from the membrane. We assume that the forward and backward rate constants are related through detailed balance

$$\beta_n = \alpha_{n-1} \exp[\tilde{F}(n) - \tilde{F}(n-1)], \quad n = 2, 3..., N, \tag{3}$$

where $\tilde{F}(n) = F(n)/(k_{_B}T)$, $F(n)$ is the formation free energy for a pit containing n monomeric units, $k_{_B}$ is the Boltzmann constant, and T is the absolute temperature.

We choose the forward rate constants to be of the form $\alpha_n = \gamma f(n, N)$, $n = 1, 2, ..., N-1$, where γ is a kinetic parameter proportional to the product of the free monomers concentration and the bimolecular association rate constant between a free monomer and a pit. The function $f(n, N)$ gives the number of available binding sites on the edge of a pit of size n. Using that the shape of a pit is a spherical cap, this function can be written as

$$f(n, N) = \rho\sqrt{n(N-n)/N}, \tag{4}$$

where ρ is a dimensionless parameter (see Appendix B).

In terms of the kinetic scheme in Fig. 3, the quantities P_w and P_f (see Eq. 1) are the probabilities that a random walk, starting from site $n = 1$, eventually reaches sites $n = N$ and $n = 0$, respectively, and the times τ_w and τ_f are the mean durations of the two processes (which formally are conditional mean first-passage times [25, 26]). Analytical expressions for these quantities are well known [25]

$$P_w = \frac{\Psi_1}{\Psi_1 + \sum\limits_{m=1}^{N} \Phi_m}, \quad P_f = 1 - P_w, \tag{5}$$

$$\tau_w = \frac{\sum\limits_{m=1}^{N} \exp[-\tilde{F}(m)] \sum\limits_{l=1}^{m} \Psi_l \sum\limits_{l=m}^{N} \Phi_l}{\Psi_1 + \sum\limits_{m=1}^{N} \Phi_m}, \tag{6}$$

$$\tau_f = \frac{\Psi_1 \sum\limits_{m=1}^{N} \exp[-\tilde{F}(m)] (\sum\limits_{l=m}^{N} \Phi_l)^2}{\sum\limits_{l=1}^{N} \Phi_l (\Psi_1 + \sum\limits_{m=1}^{N} \Phi_m)}, \tag{7}$$

where functions Ψ_n and Φ_n are given by $\Psi_n = \exp[\tilde{F}(n)]/\beta_n$ and $\Phi_n = \exp[\tilde{F}(n)]/\alpha_n$.

Free energy of pit formation

The free energy of pit formation can be written as [20, 24] (see details in Appendix C)

$$F(n, N) = E(N)n + \sigma\sqrt{n(N-n)/N}. \tag{8}$$

The free energy is mainly dominated by the first term, $E(N)n$, which is proportional to the number of monomers in the pit. It includes the costs of the membrane and protein coat distortions, entropic cost of immobilizing the monomers, and the binding energy gained due to coat formation. The second term is the line tension energy with σ being the edge-energy constant. We use a Helfrich type expression [27] for the membrane and coat distortion energy, and assume that the spontaneous curvature of the cell membrane is zero and that of the coat is finite. In addition, we assume that the binding energy and the entropic cost of immobilizing the monomers are proportional to the number of monomers in the pit. Based on these assumptions we get

$$E(N) = \frac{8\pi\kappa_m}{N} + \frac{8\pi\kappa_p}{N}\left(1 - \sqrt{\frac{N}{N_p}}\right)^2 - \epsilon_b\,, \tag{9}$$

where κ_m and κ_p are the bending rigidities of the cell membrane and the coat, respectively, N_p is the natural number of monomers in the coat - which is determined by the intrinsic coat curvature, and ϵ_b is the effective monomer binding energy, i.e., the difference between the binding energy and entropic cost.

Parameter values

The values of the parameters used in our calculation are summarized in Table II. These values, except for ϵ_b, are identical to those in Ref. 20. The rationale behind the choices is as follows: The value of κ_m typically lies between 10-25 $k_{\scriptscriptstyle B}T$ [28]; we choose $\kappa_m = 20\,k_{\scriptscriptstyle B}T$. In vitro, clathrin triskelions assemble into baskets of different sizes. The size distribution of baskets is typically narrow and has a peak close to $d_p = 90\,\mathrm{nm}$ in diameter [29]. Using the average area occupied by a clathrin molecule, $\lambda = 310\,\mathrm{nm}^2$, and the relation $\lambda N_p = \pi d_p^2$, we find that a 90 nm basket would have approximately 80 clathrin triskelions. So we choose the natural coat size to be $N_p = 80$. The value of $\lambda = 310\,\mathrm{nm}^2$ was estimated using the relation between diameters of clathrin baskets of different sizes and the number of clathrin

TABLE II: Parameter values

Parameter	Description	Value
κ_m	Membrane bending rigidity	$20\,k_{_B}T$
κ_p	Protein coat bending rigidity	$200\,k_{_B}T$
N_p	Number of monomers in a typical vesicle	80
ϵ_b	Binding energy per monomer	$10\,k_{_B}T$
σ	Edge energy constant	$2\,k_{_B}T$
γ	Kinetic parameter	$0.18\,\mathrm{sec}^{-1}$
τ_0	Average time for initiation of a CCP	$20\,\mathrm{sec}$
β_1	Backward rate constant	$0.1\,\mathrm{sec}^{-1}$
$k_{_N}$	Vesicle scission rate	∞
λ	Average area occupied by a monomer	$310\,\mathrm{nm}^2$
l_b	Length of receptor ligand bond	$15\,\mathrm{nm}$
ρ	Dimensionless parameter	2

triskelions they contain [30]. In Ref. 20, using experimental data on lifetime distribution of abortive CCPs (CCP with no cargo) we estimated the value of the effective binding energy per monomer, ϵ_b, to be approximately $5\,k_{_B}T$. Experiments show that in the presence of cargo (present case) the binding energy increases. An approximate range for its value can be determined using the following argument: for a clathrin-coated vesicle to be energetically stable, the effective binding energy has to be greater than the membrane bending energy ($8\pi\kappa_m \approx 500\,k_{_B}T$). Since a typical vesicle has 80 monomers, the binding energy per monomer should be greater than $500/80 \approx 6\,k_{_B}T$. To get an upper bound to the binding energy we consider the electrostatic binding energy between proteins containing a BAR (Bin-Amphiphysin-Rvs) domain and the membranes, which is estimated to be around $15\,k_{_B}T$ [31]. We choose a number in between these values and set $\epsilon_b = 10\,k_{_B}T$. The parameter, κ_p, captures the effective bending rigidity of the protein coat. In Ref. 20 we estimated its value to be approximately $\kappa_p = 200\,k_{_B}T$; here we use the same value. To the best of our knowledge, the value of τ_0 in the case of nanoparticles has never been measured. In the case of a particular virus (canine parvovirus) entering via clathrin-mediated endocytosis, it was found to be approximately $20\,\mathrm{sec}$ [32]. Thus we choose $\tau_0 = 20\,\mathrm{sec}$. We choose the length of

a receptor ligand bond to be $l_b = 15\,\text{nm}$ [33]. Parameters σ, ρ, and γ have the same values as in Ref. 20: $\sigma = 2\,k_BT$, $\rho = 2$, $\gamma = 0.18\,\text{sec}^{-1}$.

RESULTS

Figure 4 shows $E(N)$, Eq. 9, as a function of the NP size. It attains a minimum at $d_E^* \approx 68\,\text{nm}$, which corresponds to the size of the NP whose carrier vesicle is energetically most stable. This size can be found by solving the equation $\partial E(N)/\partial N = 0$, which leads to

$$d_E^* = (1 + \kappa_m/\kappa_p)\sqrt{\lambda N_p/\pi} - 2l_b. \tag{10}$$

For NPs larger than d_E^*, $E(N)$ increases due to the energetic cost of protein coat deformation, whereas for NPs smaller than d_E^*, $E(N)$ increases mainly due to the energetic cost of cell membrane deformation. The vertical dash-dotted lines at $d_{min} \approx 46\,\text{nm}$ and $d_{max} \approx 105\,\text{nm}$ show the NP sizes at which $E(N) = 0$. Analytical expressions of these sizes can be obtained

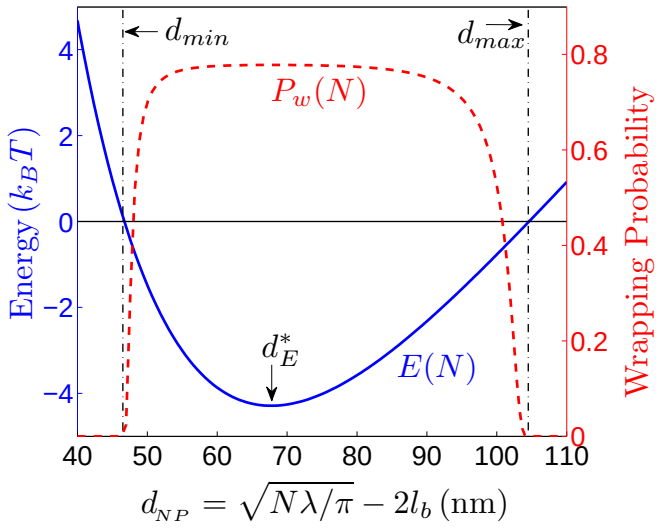

FIG. 4: Energy $E(N)$, Eq. 9, (solid curve) and the wrapping probability, $P_w(N)$, (dashed curve), as functions of the NP size. $P_w(N)$ is high when $E(N) < 0$, and pit assembly is energetically favorable. Dashed-dotted vertical lines at $d_{min} \approx 46\,\text{nm}$ and $d_{max} \approx 105\,\text{nm}$ correspond to the NP sizes at which $E(N) = 0$. The arrow at $d_E^* \approx 68\,\text{nm}$ indicates the NP size whose carrier vesicle is energetically most stable.

by solving the equation $E(N) = 0$, which leads to

$$\frac{d_{min}}{d_p} = \frac{1 - \sqrt{(1 + k'_m)\epsilon'_b - k'_m}}{(1 - \epsilon'_b)} - \frac{2l_b}{d_p}, \quad \frac{d_{max}}{d_p} = \frac{1 + \sqrt{(1 + k'_m)\epsilon'_b - k'_m}}{(1 - \epsilon'_b)} - \frac{2l_b}{d_p}, \tag{11}$$

where $\kappa'_m = \kappa_m/\kappa_p$, $\epsilon'_b = N_p\epsilon_b/8\pi\kappa_p$, and $d_p = \sqrt{\lambda N_p/\pi}$.

Figure 4 also shows the plot of the wrapping probability, $P_w(N)$. In regions where the sum of membrane and coat distortion energies is greater than the binding energy ($E(N) > 0$), pit assembly is energetically unfavorable, and $P_w(N)$ is negligibly small. In contrast, in the region where $E(N) < 0$, $P_w(N)$ rises sharply and then remains high (about 0.8) and approximately constant. Notably, sizes of several viruses which enter through clathrin-mediated endocytosis, including dengue virus (40-60 nm), semliki forest virus (50-70 nm), and reovirus (60-80 nm), fall within this range [34].

Figure 5 shows plots of the mean wrapping time, τ_w, Eq. 6, and the mean internalization time, τ, Eq. 1, as functions of the NP size. The mean wrapping time has a minimum at $d^*_w \approx 55$ nm, which is different from $d^*_E \approx 68$ nm. The difference between the two sizes is due to the NP size-dependent dynamics of coat assembly. At d^*_w, $E(N) \approx -3\, k_B T$, and hence $\alpha_n/\beta_n \approx 20 \gg 1$. This implies that coat assembly (hence NP wrapping) proceeds with a low

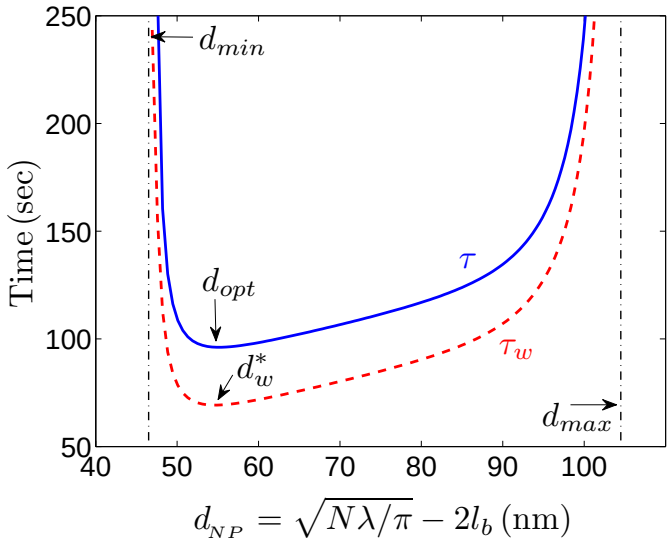

FIG. 5: Mean wrapping time, τ_w, Eq. 6, (dashed curve), and the mean internalization time, τ, calculated using Eq. 1 with $\tau_0 = 20$ sec, as functions of the NP size. Arrows at d^*_w and d_{opt} indicate the NP sizes at which τ_w and τ are minimum, respectively. Our estimate $d_{opt} \approx 55$ nm matches well with experimental observations presented in Table I.

probability of monomer dissociation. As a consequence, the wrapping time is determined by the rate of arrival of a new monomer. For NPs larger than d_w^*, up to approximately 85 nm, the inequality $\alpha_n/\beta_n \gg 1$ holds true, but the number of monomers needed to wrap a NP increases. As a consequence, the wrapping time increases with NP size. For NPs larger than 85 nm, the dissociation of monomers becomes more frequent, which causes the wrapping time to increase drastically. For NPs smaller than d_w^*, the free energy $E(N)$ rises sharply, and, therefore, the rate constants α_n and β_n become comparable. Thus, even though the number of monomers needed to wrap a NP decreases, the wrapping time increases due to frequent dissociation of the monomers. The mean time of failed attempts, τ_f, given in Eq. 7, shows a trend very similar to that of τ_w, but its values are almost an order of magnitude smaller.

In Fig. 5 we show the mean internalization time, τ, calculated using Eq. 1 with $\tau_0 = 20$ sec. The mean internalization time includes the mean wrapping time, τ_w, and the mean time spent by the NP in failed attempts. In the region where P_w is high and almost constant (see Fig. 4), we find $P_w\tau_w \gg P_f\tau_f$. Equation 1 then simplifies to $\tau \approx (\tau_0/P_w) + \tau_w$, and τ is just the mean wrapping time, τ_w, shifted by a constant τ_0/P_w. When d_{NP} is close to d_{min} or d_{max}, P_w drops sharply and, therefore, τ increases more rapidly than τ_w. The mean internalization time has a minimum at d_{opt}, which corresponds to the NP size at which the cellular uptake of the NPs is the fastest. Our analysis predicts $d_{opt} \approx 55$ nm, which is close to the optimal NP size observed in different experiments (see Table 1). In the case of NPs, the size dependence of internalization times at a single NP level has never been measured, therefore a direct comparison of our results with with experimental data is not possible. However, internalization times of some viruses and virus-like particles entering into cells via clathrin-mediated endocytosis have been measured to be in the range 50-400 sec [21, 32, 35, 36], which agrees with our analysis.

Finally, we look at sensitivity of our results to variations in coat parameter values. In Fig. 6 we show plots of d_{min}, d_{max}, d_{opt}, and d_E^* as functions of the parameters κ_p, ϵ_b, and N_p. The dependence of the optimal size, d_{opt}, on the coat parameters has been determined numerically, while other dependences are are given by Eqs. 10 and 11. Only the maximum NP size, d_{max}, shows appreciable variation; the other quantities show weak dependences on the coat parameters. This demonstrates that our main results are stable with respect to small variations in the coat parameters around their chosen values.

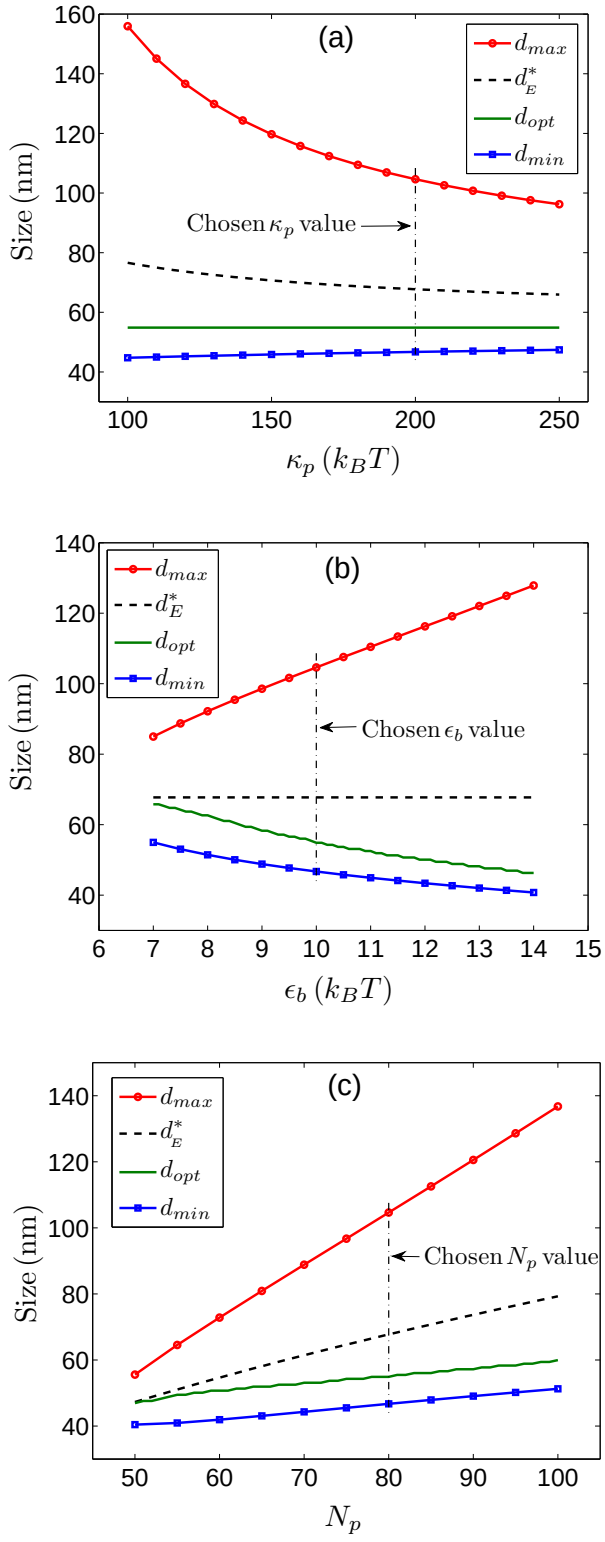

FIG. 6: Plots of d_{min}, d_{max} (Eq. 11), d_E^* (Eq. 10), and d_{opt} (calculated numerically), as functions of (a) κ_p - the bending rigidity of the protein coat (b) ϵ_b - effective monomer binding energy, and (c) N_p - natural number of monomers in the coat. The vertical dash-dotted line in each case shows the parameter value used in our calculations. The plot shows that our results for d_{min}, d_E^*, and d_{opt} are stable with respect to small variations in the parameter values. Only the maximum NP size d_{max} shows significant variation.

SUMMARY AND DISCUSSION

In this study we investigated how the assembly of the protein coat on the cytoplasmic side of the plasma membrane affects the cellular uptake of NPs. To address this question we have used a previously developed model of clathrin-coated vesicle formation. We have used the mean internalization time of a NP, τ, as the measure of its internalization efficiency, and calculated the dependence of τ on the NP size. We found that the NP size has lower and upper boundaries (d_{min} and d_{max}) at which the internalization time becomes very large, i.e., beyond these sizes, internalization via clathrin-mediated endocytosis is highly improbable. We also found that there is an optimal NP size d_{opt} at which the internalization time is a minimum. All these sizes are determined by the parameters of the coat assembly process.

As described earlier, d_{opt} is determined by the dynamics of coat assembly. Since the coat parameters do not change appreciably between different cells and are also independent of the details of the NP design, an explanation for why the same optimal size was observed in different experiments (see Table I) follows naturally from our analysis. In contrast, this observation is difficult to rationalize using previous models which predict that optimal size depends on the ligand density on the NP, the density of the corresponding receptors on the cell membrane, and the receptor-ligand binding energy [12–14], since these parameters can vary significantly depending on the cell line and ligand used in the experiment.

Our calculation of the smallest NP size, $d_{min} \approx 46\,\text{nm}$, is based on the assumption that the size of the NP is related to the size of its carrier vesicle through $d_V^{min} = d_{min} + 2l_b$, which gives $d_V^{min} \approx 76\,\text{nm}$. In principle, however, NPs with diameter slightly smaller than d_{min} can be internalized in a vesicle of size d_V^{min}. Also, it has been shown that NPs much smaller than d_{min} can be internalized in clusters (multiple particles per vesicle), in a vesicle of size much larger than the size of individual NPs [19]. Therefore, a comparison of d_{min} with experimental data is meaningless. In this case it is more meaningful to compare d_V^{min} with the size of the smallest clathrin-coated vesicles. Experimentally observed size of smallest clathrin-coated vesicles is approximately 70 nm in diameter [37], which agrees very well with our estimate.

Our estimate of the largest NP size, $d_{max} \approx 105\,\text{nm}$, and the size of its carrier vesicle, $d_V^{max} \approx 105 + 30 = 135\,\text{nm}$, are smaller than their corresponding experimentally measured values 200 nm [4, 5], and 200 nm [37], respectively. As shown in Fig. 6 the value of d_{max}

is sensitive to the coat parameter values. By changing their values slightly we can get d_{max} close to experimentally observed values, while keeping d_{opt} the same. For example, for $\kappa_p = 150 k_B T$ and $\epsilon_b = 12 k_B T$, we get $d_{max} = 140\,\text{nm}$, $d_V^{max} = 170\,\text{nm}$, $d_{min} = 40\,\text{nm}$, and $d_{opt} = 50\,\text{nm}$. However, in this paper our aim is not to match the different sizes precisely, but rather to see the extent to which our previously developed model can explain the size dependence of NP uptake without changing the parameter values. Considering the fact that most of the parameters were determined in a completely different context (by fitting lifetime distribution of abortive CCPs) we think that such a disparity is acceptable. As mentioned earlier, other models that do not take coat assembly into consideration, incorrectly predict that very large (micron size) NPs can be internalized via receptor-mediated endocytosis [12, 13].

Although in our model the density of ligands on a NP, the receptor density on the cell membrane, and the receptor-ligand binding energy do not appear explicitly, these factors do enter our model implicitly. For example, our initial assumption that the dissociation of the NP from the membrane can be neglected would hold true only if either the receptor-ligand binding energy is strong, or the ligand and receptor densities are large enough so that a NP quickly attaches to the cell membrane by multiple receptor-ligand bonds. Multiple bonds lead to an increased lifetime of NPs on the cell membrane [38, 39]. Also, it has been shown that CCP assembly is triggered when there is receptor clustering [40] which, for our model, implies that a few receptor-ligand bonds probably have to form before the first monomer can arrive. Thus, the time τ_0 might be affected by the above mentioned parameters.

Experimentally, the question of how the ligand density on a NP and receptor density on cell membrane affect cellular uptake is not clearly understood. It has been observed that increasing the ligand density increases cellular uptake due to an enhanced residence time of the NP on the cell membrane, and not due to an increase in the internalization rate [38]. This observation is consistent with our hypothesis that the internalization time is determined by the kinetics of coat assembly. The overall picture of NP internalization proposed in our model can be tested experimentally with total internal reflection fluorescence (TIRF) microscopy. Using dual color TIRF, where both NPs and CCPs are fluorescent, uptake of NPs at a single particle level can be monitored. This will allow simultaneous measurements of τ_0, τ_w, and τ.

To conclude we show that several experimental observations related to size dependent

cellular uptake of NPs, including the optimal NP size, can be understood to be consequences of the protein coat assembly process. Therefore, future efforts on modeling endocytosis of NPs and designing NPs for biomedical applications must take the effect of the protein coat assembly explicitly into consideration.

APPENDICIES

Appendix A: Mean internalization time τ

Here we derive the expression for the mean internalization time τ given in Eq. 1. This time is defined as the average time between the NP binding to the cell membrane and its internalization, assuming that the binding is irreversible. Consider an ensemble of NP-receptor complexes formed on the cell membrane at time $t = 0$. The mean internalization time τ can be written as

$$\tau = P_w(\tau_0 + \tau_w) + P_f P_w(2\tau_0 + \tau_f + \tau_w) + P_f^2 P_w(3\tau_0 + 2\tau_f + \tau_w) + ... \tag{12}$$

The first term in right hand side of this equality is the contribution from the fraction (P_w) of complexes which are internalized on the first attempt, i.e., the complexes which bind to coat protein and get internalized. The second term is the contribution from the fraction ($P_f P_w$) of complexes that are internalized on the second attempt, i.e., they bind to coat proteins, dissociate from them, bind to coat protein for the second time, and then get internalized. Subsequent terms can be understood in the same way. Upon summing the series, we obtain

$$\tau = (\tau_0 + P_w\tau_w + P_f\tau_f)/P_w\,. \tag{13}$$

This expression for the mean internalization time τ can be written in the form given in Eq. 1.

Appendix B: Derivation of $f(n)$ in Eq. 4

Using spherical coordinates (see Fig.7) the surface area of the pit can be written as

$$A(\theta) = 2\pi R^2[1 - \cos(\theta)] = \lambda n, \tag{14}$$

where R is the radius of a sphere having the same curvature as the pit. This leads to the relation between $\cos(\theta)$ and the number of monomers, n, in the pit,

$$\cos(\theta) = 1 - \frac{\lambda n}{2\pi R^2}\,. \tag{15}$$

From the above equation, we thus infer that the radius, $r(n)$, of the circular growing edge of a pit is

$$r(n) = R\sin(\theta) = R\sqrt{[1+\cos(\theta)][1-\cos(\theta)]} = \sqrt{\left(\frac{\lambda n}{\pi}\right)\left(1-\frac{\lambda n}{4\pi R^2}\right)}. \tag{16}$$

Introducing the average linear span of the monomer, denoted by L, we find that the number of available binding sites on the periphery of the pit is

$$f(n) = \frac{2\pi r(n)}{L} = \frac{2\pi}{L}\sqrt{\left(\frac{\lambda n}{\pi}\right)\left(1-\frac{\lambda n}{4\pi R^2}\right)}. \tag{17}$$

By changing variables from R to N using the relation $4\pi R^2 = \lambda N$, we arrive at

$$f(n) = \rho\sqrt{n(N-n)/N}, \tag{18}$$

where ρ is a dimensionless parameter given by $\rho = \sqrt{4\pi\lambda/L^2}$.

Appendix C: Derivation of $F(n)$ in Eq. 8

The formation free energy of a pit made of n monomers and having a curvature c can be written as

$$F(n,c) = 2\kappa_m\lambda n c^2 + 2\kappa_p\lambda n(c-c_p)^2 - \epsilon_b n + \sigma f(n,c). \tag{19}$$

The first term is the Helfrich energy [27] describing the energetic cost of bending the cell membrane assuming that its spontaneous curvature is zero. The second term represents the

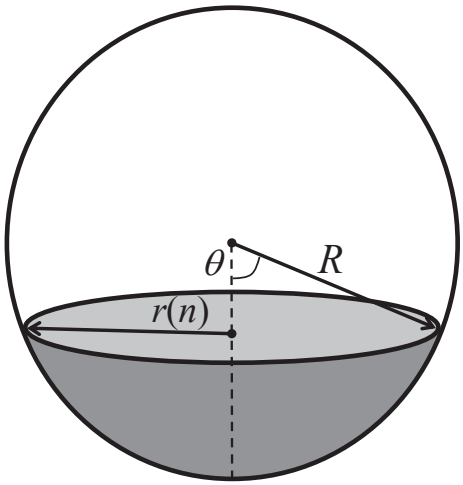

FIG. 7: Spherical cap model of a pit.

bending energy of the protein coat, with c_p being the spontaneous curvature of the coat. The third term represents the effective binding energy. The fourth term is the line tension energy. By changing variables from c to N and c_p to N_p using the relations $4\pi/c^2 = \lambda N$ and $4\pi/c_p^2 = \lambda N_p$, we arrive at the expression for the free energy of the pit formation given in Eq. 8.

ACKNOWLEDGMENTS

This study was supported by the Intramural Research Program of the National Institutes of Health (NIH) – *Eunice Kennedy Shriver* National Institute of Child Health and Human Development, and the Center for Information Technology.

---

[1] Sahoo, S. K., and V. Labhasetwar, 2003. Nanotech approaches to drug delivery and imaging. Drug Discov. Today 8:1112–1120.

[2] Bareford, L. M., and P. W. Swaan, 2007. Endocytic mechanisms for targeted drug delivery. Adv. Drug Deliv. Rev. 59:748–758.

[3] Akinc, A., and G. Battaglia, 2013. Exploiting endocytosis for nanomedicines. Cold Spring Harb Perspect Biol 5:a016980.

[4] Rejman, J., V. Oberle, I. S. Zuhorn, and D. Hoekstra, 2004. Size-dependent internalization of particles via the pathways of clathrin- and caveolae-mediated endocytosis. Biochem. J. 377:159–169.

[5] Oh, J.-M., S.-J. Choi, G.-E. Lee, J.-E. Kim, and J.-H. Choy, 2009. Inorganic metal hydroxide nanoparticles for targeted cellular uptake through clathrin-mediated endocytosis. Chem. Asian J. 4:67–73.

[6] Osaki, F., T. Kanamori, S. Sando, T. Sera, and Y. Aoyama, 2004. A quantum dot conjugated sugar ball and its cellular uptake. On the size effects of endocytosis in the subviral region. J. Am. Chem. Soc. 126:6520–6521.

[7] Chithrani, B. D., A. A. Ghazani, and W. C. W. Chan, 2006. Determining the size and shape dependence of gold nanoparticle uptake into mammalian cells. Nano. Lett. 6:662–668.

[8] Wang, S. H., C.W. Lee, A. Chiou, and P.-K. Wei, 2010. Size-dependent endocytosis of

gold nanoparticles studied by three-dimensional mapping of plasmonic scattering images. J. Nanobiotechnology 8:33.

[9] Lu, F., S. H. Wu, Y. Hung, and C.-Y. Mou, 2009. Size effect on cell uptake in well-suspended, uniform mesoporous silica nanoparticles. Small 5:1408–1413.

[10] Albanese, A., and W. C. W. Chan, 2011. Effect of gold nanoparticle aggregation on cell uptake and toxicity. ACS Nano 5:5478–5489.

[11] Andar, A. U., R. R. Hood, W. N. Vreeland, D. L. Devoe, and P. W. Swaan, 2013. Microfluidic Preparation of Liposomes to Determine Particle Size Influence on Cellular Uptake Mechanisms. Pharm. Res.

[12] Gao, H., W. Shi, and L. B. Freund, 2005. Mechanics of receptor-mediated endocytosis. Proc. Natl. Acad. Sci. USA 102:9469–9474.

[13] Zhang, S., J. Li, G. Lykotrafitis, G. Bao, and S. Suresh, 2009. Size-Dependent Endocytosis of Nanoparticles. Adv. Matter 21:419–424.

[14] Yuan, H., J. Li, G. Bao, and S. Zhang, 2010. Variable nanoparticle-cell adhesion strength regulates cellular uptake. Phys. Rev. Lett. 105:138101.

[15] Decuzzi, P., and M. Ferrari, 2007. The role of specific and non-specific interactions in receptor-mediated endocytosis of nanoparticles. Biomaterials 28:2915–2922.

[16] Mirigian, S., and M. Muthukumar, 2013. Kinetics of particle wrapping by a vesicle. J. Chem. Phys. 139:044908.

[17] Mousavi, S. A., L. Malerød, T. Berg, and R. Kjeken, 2004. Clathrin-dependent endocytosis. Biochem. J. 377:1–16.

[18] Ungewickell, E. J., and L. Hinrichsen, 2007. Endocytosis: clathrin-mediated membrane budding. Curr. Opin. Cell Biol. 19:417–425.

[19] Chithrani, B. D., and W. C. W. Chan, 2007. Elucidating the mechanism of cellular uptake and removal of protein-coated gold nanoparticles of different sizes and shapes. Nano Lett. 7:1542–1550.

[20] Banerjee, A., A. Berezhkovskii, and R. Nossal, 2012. Stochastic model of clathrin-coated pit assembly. Biophys. J. 102:2725–2730.

[21] Ehrlich, M., W. Boll, A. V. Oijen, R. Hariharan, K. Chandran, M. L. Nibert, and T. Kirchhausen, 2004. Endocytosis by random initiation and stabilization of clathrin-coated pits. Cell 118:591–605.

[22] Loerke, D., M. Mettlen, D. Yarar, K. Jaqaman, H. Jaqaman, G. Danuser, and S. L. Schmid, 2009. Cargo and dynamin regulate clathrin-coated pit maturation. PLoS Biol. 7:e57.

[23] Liu, J., Y. Sun, D. G. Drubin, and G. F. Oster, 2009. The mechanochemistry of endocytosis. PLoS Biol. 7:e1000204.

[24] Foret, L., and P. Sens, 2008. Kinetic regulation of coated vesicle secretion. Proc. Natl. Acad. Sci. USA 105:14763–14768.

[25] Van Kampen, N., 2011. Stochastic Processes in Physics and Chemistry. North-Holland Personal Library. Elsevier Science.

[26] Redner, S., 2001. A Guide to First-Passage Processes. A Guide to First-passage Processes. Cambridge University Press.

[27] Helfrich, W., 1973. Elastic properties of lipid bilayers: theory and possible experiments. Z. Naturforsch. C. 28:693–703.

[28] Boal, D., 2002. Mechanics of the Cell. Cambridge University Press.

[29] Zaremba, S., and J. H. Keen, 1983. Assembly polypeptides from coated vesicles mediate reassembly of unique clathrin coats. J. Cell Biol. 97:1339–1347.

[30] Nossal, R., 2001. Energetics of clathrin basket assembly. Traffic 2:138–147.

[31] Parthasarathy, R., C. han Yu, and J. T. Groves, 2006. Curvature-modulated phase separation in lipid bilayer membranes. Langmuir 22:5095–5099.

[32] Cureton, D. K., C. E. Harbison, E. Cocucci, C. R. Parrish, and T. Kirchhausen, 2012. Limited transferrin receptor clustering allows rapid diffusion of canine parvovirus into clathrin endocytic structures. J. Virol. 86:5330–5340.

[33] Bell, G. I., M. Dembo, and P. Bongrand, 1984. Cell adhesion. Competition between nonspecific repulsion and specific bonding. Biophys. J. 45:1051–1064.

[34] Mudhakir, D., and H. Harashima, 2009. Learning from the viral journey: how to enter cells and how to overcome intracellular barriers to reach the nucleus. AAPS. J. 11:65–77.

[35] Rust, M. J., M. Lakadamyali, F. Zhang, and X. Zhuang, 2004. Assembly of endocytic machinery around individual influenza viruses during viral entry. Nat. Struct. Mol. Biol. 11:567–573.

[36] de Bruin, K., N. Ruthardt, K. von Gersdorff, R. Bausinger, E. Wagner, M. Ogris, and C. Bräuchle, 2007. Cellular dynamics of EGF receptor-targeted synthetic viruses. Mol. Ther. 15:1297–1305.

[37] Kirchhausen, T., 2009. Imaging endocytic clathrin structures in living cells. Trends Cell Biol.

19:596–605.

[38] Hong, S., P. R. Leroueil, I. J. Majoros, B. G. Orr, J. R. Baker, and M. M. B. Holl, 2007. The binding avidity of a nanoparticle-based multivalent targeted drug delivery platform. Chem. Biol. 14:107–115.

[39] Jiang, W., B. Y. S. Kim, J. T. Rutka, and W. C. W. Chan, 2008. Nanoparticle-mediated cellular response is size-dependent. Nat. Nanotechnol. 3:145–150.

[40] Liu, A. P., F. Aguet, G. Danuser, and S. L. Schmid, 2010. Local clustering of transferrin receptors promotes clathrin-coated pit initiation. J. Cell Biol. 191:1381–1393.